Normal-Mode Global Rossby Waves: Theory and Observations

JON E. AHLQUIST[1]

Center for Climatic Research, and Department of Meteorology, University of Wisconsin-Madison 53706

(Manuscript received 12 March 1981, in final form 3 November 1981)

ABSTRACT

This study addresses first the question of what normal-mode global Rossby waves might exist in the Earth's atmosphere. Then it identifies fourteen of these theoretically predicted waves in the NMC global tropospheric analyses.

Normal modes of linearized global primitive shallow water equations were found given a basic state of latitudinally dependent steady zonal flow. The solutions are free Rossby and gravity waves. Many of the waves' north–south structures are similar to Hough functions, which are the solutions of the simpler problem of free waves in an atmosphere at rest.

By projecting 1200 consecutive days of twice-daily NMC global tropospheric analyses of velocity and geopotential onto idealized three-dimensional, normal-mode Rossby wave structures, time series of wave amplitudes and phases were formed. Spectral analyses of these time series for zonal wavenumbers 1–4 revealed statistically significant peaks at eight out of 25 theoretical Rossby wave frequencies. Six additional waves may exist, but their significance could not be statistically supported because their spectral peaks fell into the red noise portion of the spectra. Periods for the fourteen waves lie between ~2 and ~30 days. Excluding the two weakest waves, average amplitudes at the surface range from 0.3 to 2 mb.

Prior to this study, only two normal-mode Rossby waves had been identified with confidence in the troposphere, a zonal wavenumber-1, 5-day wave and a zonal wavenumber-1, 16-day wave. This study has identified up to ten more modes which have comparable amplitudes.

1. Introduction

Planetary-scale waves are important because they determine large-scale temperature and wind regimes and hence also storm tracks. Among studies of planetary waves, few have dealt with the normal modes of the atmosphere. Normal modes are free waves; within a linearized approach, their speeds and structures are determined by the resonant characteristics of the mean state of the atmosphere rather than by forcing mechanisms.

Madden (1979) has reviewed the theory and observations of planetary-scale free Rossby waves, and Daley (1981) has reviewed the use of normal modes to initialize numerical models. Therefore, only highlights will be noted here. Haurwitz (1940) theoretically studied horizontally nondivergent, free Rossby waves in an atmosphere in solid body rotation. This is a particular case from Laplace tidal theory (Longuet-Higgins, 1968; Kasahara, 1976) which has an analytical solution. The horizontal dependence of the streamfunction of such a Rossby wave is proportional to a spherical harmonic, and the wave's angular velocity is given by a simple formula.

Eliasen and Machenhauer (1965) looked for some of the waves predicted by this nondivergent Laplace tidal theory. They decomposed Northern Hemisphere 500 and 1000 mb streamfunctions into spherical harmonics for a 90-day winter period and followed the amplitudes and phases of these components. Their Figs. 3 and 4 show six modes whose speeds are qualitatively consistent with Haurwitz's theoretical results. Eliasen and Machenhauer were able to bring theoretical wave speeds into closer agreement with observations by using a model which parametrically allowed for horizontally divergent motion. This produced the desirable effect of reducing the faster theoretical speeds. [See also Dikii and Golitsyn (1968) and Eliasen and Machenhauer (1969).]

Two of the free modes tentatively identified by Eliasen and Machenhauer (1965) have been more thoroughly studied. Both are zonal wavenumber-one waves. One has a five-day period and an average amplitude at the surface of 0.25 mb in the tropics and 0.5–1.0 mb in mid-latitudes (Madden and Julian, 1972, 1973; Madden, 1978). It has been correlated with precipitation in the tropical Atlantic (Burpee, 1976) and Pacific (Yanai *et al.*, 1976).

The other mode to receive more intensive study has an observed period of ~16 days and an average surface amplitude of ~5 mb at 60°N during winter (Madden, 1978; see also Sato, 1977). According to

[1] Present affiliation: Department of Meteorology, Florida State University, Tallahassee, FL 32306.

0022-4928/82/020193-10$06.50

Laplace tidal theory, this mode should be equally strong in the Southern Hemisphere, but Madden (1978) was unable to detect coherence between geopotential time series for 60°N and 60°S at periods near 16 days. This asymmetric response with respect to the equator means that, if this wave is a free mode (as is likely), it must be modeled in a basic state which itself is asymmetric with respect to the equator. [As Madden (1978, p. 1616) noted, critical latitude trapping is unlikely for this mode].

The purpose of the present study is to extend the classical Laplace tidal model for normal modes as well as Eliasen and Machenhauer's (1965) observational search for these theoretical modes. In section 2, we pose the free mode problem for a global shallow water model with a basic state which can be asymmetric with respect to the equator, and we discuss numerical methods for solving the problem. In section 3, the free Rossby modes of this model are examined. In section 4, results of a search for free Rossby modes are presented. Section 5 is an overview.

2. The generalized Laplace tidal equation

Normal-mode Rossby waves were modeled using the global, primitive, shallow water equations. This same model was studied independently by Kasahara (1980). The shallow water equations are first linearized about a basic state of steady, latitudinally dependent zonal flow. The basic state zonal flow, u_0, and free surface height, h_0, are constrained by the meridional equation of motion,

$$\frac{\partial H_0}{\partial \theta} = \bar{\omega}(\bar{\omega} + 1)\gamma^{-2} \sin\theta \cos\theta, \tag{1}$$

where

$$\left.\begin{aligned} H_0 &= h_0(\theta)/h_e \\ \bar{\omega} &= u_0(\theta)/(2a\Omega \sin\theta) \\ \gamma &= (gh_e)^{1/2}/(2a\Omega) \end{aligned}\right\}. \tag{2}$$

Colatitude $\theta = 90° -$ latitude is used as the meridional coordinate instead of latitude because spectrally expanded solutions to the upcoming perturbation equations are more simply written using colatitude. The vertical scaling length h_e is called the equivalent depth and is taken to be 10 km. (See Kasahara, 1976; Salby, 1979.) Values for physical constants are chosen to agree with Kasahara (1976), i.e. $g = 9.8$ N kg^{-1}, $a = (20\ \pi^{-1}) \times 10^6$ m, and $\Omega = 2\pi/(60 \times 60 \times 24)$ rad s^{-1}. Thus, $\gamma = 0.338$.

After specifying a zonal wind profile $u_0(\theta)$, we compute $\bar{\omega}$ by (2) and then H_0 by numerically integrating (1) using Simpson's rule. The constant of integration is chosen so that the global average of H_0 is one. This makes the atmospheric mass independent of the zonal wind profile and dependent only on the equivalent depth h_e.

Next, we assume that the perturbation velocity and free surface height can be written as:

$$\left.\begin{bmatrix} u' \\ v' \\ h' \end{bmatrix} = \mathrm{Re}\left\{\begin{bmatrix} (gh_e)^{1/2} & U(\theta) \\ -i(gh_e)^{1/2} & V(\theta) \\ h_e & H(\theta) \end{bmatrix} W_0 \times \exp[i(s\lambda - 2\Omega\sigma t)]\right\}\right. . \tag{3}$$

Following meteorological convention, u' and v' are the eastward and northward components, respectively, of the perturbation velocity. Re means the real part, $i = (-1)^{1/2}$, W_0 is the nondimensional complex wave amplitude, s is the zonal wavenumber, λ is longitude, and σ is the nondimensional wave frequency. We restrict s to positive integers so that a negative (positive) frequency indicates a westward (eastward) traveling wave.

With this separation of variables, the perturbation equations of motion and continuity equation can be written in matrix form as

$$\mathsf{L}\mathsf{F} = \sigma\mathsf{F}$$

where

$$\mathsf{L} \equiv \begin{bmatrix} s\bar{\omega} & \left[(1 + 2\bar{\omega})\cos\theta + \left(\frac{d\bar{\omega}}{d\theta}\right)\sin\theta\right] & \frac{s\gamma}{\sin\theta} \\ (1 + 2\bar{\omega})\cos\theta & s\bar{\omega} & -\gamma\frac{d}{d\theta} \\ \frac{s\gamma H_0}{\sin\theta} & \gamma\left[H_0\left(\frac{d}{d\theta} + \cot\theta\right) + \frac{dH_0}{d\theta}\right] & s\bar{\omega} \end{bmatrix}, \tag{4}$$

and

$$\mathsf{F} \equiv \begin{bmatrix} U \\ V \\ H \end{bmatrix}.$$

If one were to set $\bar{\omega} = 0$ (so then $H_0 = 1$ everywhere), (4) would be the classical Laplace tidal equation. Therefore, we shall refer to (4) as the generalized Laplace tidal equation.

Next, we specify the normalization for F. Define the inner product between vectors F_α and F_β as:

$$\langle \mathsf{F}_\alpha, \mathsf{F}_\beta \rangle = \int_0^\pi [H_0(U_\alpha U_\beta^* + V_\alpha V_\beta^*) + H_\alpha H_\beta^*] \sin\theta \, d\theta, \quad (5)$$

where the asterisk indicates the complex conjugate. The normalization for eigenfunction F is:

$$\langle \mathsf{F}, \mathsf{F} \rangle = 1. \quad (6)$$

This sets the latitudinally-dependent portion of a wave's kinetic energy plus available potential energy equal to a constant. It is analogous to the normalization often used for the classical Laplace tidal problem.

Orszag (1974, pp. 60, 65) has reviewed polar boundary conditions. With the numerical methods used by the author, kinematic velocity constraints (Orszag, p. 65) were not necessary. See Boyd (1978) for examples of other polar constraints which are not always needed.

Because of discrepancies [which have since been resolved (Kasahara, 1981)] between the author's results and those of Kasahara (1980), the author solved the generalized Laplace tidal equation using several independent finite difference and spectral techniques. All the methods produced spurious eigenfrequencies and eigenfunctions which were identified by extreme lack of smoothness in the eigenfunctions and by lack of repeatability when the number of grid points or spectral terms was varied. Two of the methods deserve individual mention.

The second-order centered finite difference method, used by Dickinson and Williamson (1972) in their related study, was programmed easily and produced moderately accurate results with the following proviso. The continuity equation contains the divergence term

$$(\sin\theta)^{-1} d(V \sin\theta)/d\theta = (dV/d\theta + V \cot\theta).$$

When this term was approximated as

$$(\sin\theta_j)^{-1}(V_{j+1} \sin\theta_{j+1} - V_{j-1} \sin\theta_{j-1})/(2\Delta\theta), \quad (7)$$

computed eigenfunctions were smooth, but use of

$$[(V_{j+1} - V_{j-1})/(2\Delta\theta) + V_j \cot\theta_j] \quad (8)$$

produced jagged eigenfunctions.

The collocation (or "pseudospectral") method (Orszag, 1974; Boyd, 1978) was the author's preference among all the methods tried. It was accurate, easy to program, and economical. The latitudinal dependences of the perturbation velocity and free surface height were expanded as

$$\left.\begin{aligned}(U, V) &= \sum_{n=0}^{N-1} (U_n, V_n) \sin^{|k-1|}\theta \cos n\theta \\ H &= \sum_{n=0}^{N-1} H_n \sin^k\theta \cos n\theta\end{aligned}\right\}, \quad (9)$$

where $k = 0$ (1) for even (odd) zonal wavenumber. (See Orszag, 1974, sections 3 and 7). The collocation points were $\theta_j = \pi(j - \frac{1}{2})/N$, $j = 1, \ldots, N$. The generalized matrix eigenvalue problem, $\mathsf{Ax} = \sigma\mathsf{Bx}$, which resulted from applying the collocation method, was solved directly by subroutine RGG from the EISPACK eigensystem package. The solutions shown in the next section were computed in single precision on a Univac 1100/82 computer, using the collocation method with $N = 25$.

3. Rossby wave solutions of the generalized Laplace tidal equation

The normal modes of the generalized Laplace tidal problem posed in the previous section include eastward and westward traveling gravity waves as well as Rossby waves, but our interest is restricted to the latter case. A normal mode Rossby wave will be indexed by its zonal wavenumber s and a meridional index l_R defined as the number of zeros in the wave's meridional velocity profile. (Zeros at the poles are not included in the tally for l_R.) Dickinson and Williamson (1972) and Kasahara (1980) both followed this indexing scheme. Others, such as Eliasen and Machenhauer (1965, 1969), Madden (1978, 1979), and Schoeberl and Clark (1980), indexed modes using the zonal wavenumber and the parameter $n = s + l_R$.

a. Eigenvalues

The free-mode frequencies of a moving basic state differ from those of a resting basic state for a number of reasons. For example, the frequency formula for nondivergent Rossby waves derived by Haurwitz (1940) shows that putting an atmosphere into solid-body rotation does not simply Doppler-shift all the wave speeds by the solid-body rotation rate. There is also an opposing Coriolis effect, which approaches zero as $s + l_R$ increases. Kasahara (1980) has derived an approximate frequency formula for the generalized Laplace tidal equation which includes additional effects due to non-solid rotation.

Table 1 lists some of the discrete free Rossby-mode frequencies of the generalized Laplace tidal equation given the average December, January, February 500 mb zonal wind profile from Kasahara (1980) as the basic state. (Henceforth, this will be referred to as the DJF basic state.) Note that 4–5 days is the period for $l_R = 1$ waves, 7–10 days for $l_R = 2$, 14–20 days

TABLE 1. Frequencies (in cycles day^{-1}) of Rossby-wave normal modes of the generalized Laplace tidal equation given the DJF basic state. The negative signs indicate westward propagation.

s	$l_R = 0$	1	2	3	4	5	6
1	−0.83	−0.21	−0.10	−0.05	−0.04	−0.02	−0.015
2	−0.58	−0.26	−0.14	−0.07	−0.05	−0.03	−0.02
3	−0.43	−0.23	−0.14	−0.07	−0.05	−0.04	
4	−0.34	−0.19	−0.12	−0.07	−0.05		

TABLE 2. Frequencies (in cycles day^{-1}) of resonant Rossby waves in the linearized, quasi-geostrophic, global model of Schoeberl and Clark (1980) given a January basic state. The negative signs indicate westward propagation.

s						
1	−0.17	−0.07	−0.024	−0.02	−0.012	
2	−0.18	−0.09	−0.05	−0.03	−0.02	
3	−0.17	−0.08	−0.04	−0.03	−0.02	−0.014

for $l_R = 3$, etc. No frequency appears in Table 1 for ($s = 3$, $l_R = 6$), ($s = 4$, $l_R = 5$), and ($s = 4$, $l_R = 6$) because there are no free modes in the discrete spectrum having those indices.

Table 2 lists the free-mode frequencies found by Schoeberl and Clark (1980) using a multi-level quasi-geostrophic model with a January basic state. Gaps have been left before and after the first frequency for each wavenumber because, as shown in Table 1, the shallow water theory gives frequencies which occupy these gaps. Note also that the frequencies in the first column of Table 2 are lower than the $l_R = 1$ frequencies in Table 1. Moura (1976, Fig. 9) has observed that free mode frequencies for odd l_R are underestimated somewhat if the balance equations are used instead of primitive equations, and this is caused by inaccurate modeling of horizontal divergence effects by the balance equations. This may hold for the quasi-geostrophic equations as well. However, an explanation of all the differences between Tables 1 and 2 is not a simple matter. The generalized Laplace tidal model uses primitive equation dynamics, but it has only one layer. Schoeberl and Clark's model uses quasi-geostrophic dynamics, which are not ideal for global problems, but it has many vertical levels, which allow for a much more realistic basic state and more degrees of freedom in the free mode response, e.g., internal modes are possible. Also, dissipation in Schoeberl and Clark's model obviates numerical problems with critical latitudes.

b. *Eigenfunctions*

The nondimensional eigenfunctions corresponding to the eigenfrequencies in Table 1 are displayed in Fig. 1. Also shown in Fig. 1 are the eigenfunctions for a resting basic state; these are Hough functions. Differences between the two sets of eigenfunctions are small for $s + l_R$ small and increase as $s + l_R$ increases. This same result was observed when other basic states typical of tropospheric conditions were imposed. Thus, the north-south structure of free Rossby modes seems to be only weakly dependent on the basic state when $s + l_R$ is small. A qualitative feel for the weak dependence on the basic state can be gained by looking at the generalized Laplace tidal equation and noting that those terms which also appear in the classical Laplace tidal equation are often an order of magnitude larger than the additional terms due to a moving basic state.

The theoretical global structures of the waves ($s = 1$, $l_R = 1$) and ($s = 1$, $l_R = 3$) given the DJF basic state are sketched in Fig. 2. These modes are almost certainly the waves deduced by Madden (1978). Sketches of the other waves whose latitudinal structures are graphed in Fig. 1 have been omitted for reasons of space. However, the reader can make such a sketch for a wave of interest by first drawing the high and low pressure centers from the information in Fig. 1 and then adding the velocity field using the fairly good approximation of geostrophic flow outside of the tropics if $l_R \geq 1$. (This is easier than using the velocity information which is explicitly given in Fig. 1.) There is also some cross-isobaric flow which is required by the continuity equation in order that the geopotential field may move.

Fig. 3 shows the nondimensional latitudinal dependence of the geopotential for the ($s = 1$, $l_R = 3$) eigenfunction given the DJF and JJA (June, July, August 500 mb zonal average) basic states. The eigenfunction is asymmetric with respect to the equator given either basic state, the geopotential being not quite a factor of two smaller in the summer hemisphere. However, it is questionable whether a factor of two could explain the lack of coherence between 60°N and 60°S at periods near 16 days which was reported by Madden (1978). Inclusion of realistic vertical shear in the basic state, as was done by Schoeberl and Clark (1980), further accentuates Northern/Southern Hemisphere asymmetry in the free mode response, and this may be sufficient to account for Madden's observation.

Neither the present shallow water model nor Schoeberl and Clark's model can fully explain why the 16-day wave is most prominent in the Northern Hemisphere during the winter season. This matter involves not only the response to the seasonal basic state, as suggested by Fig. 3, but also dissipation (Salby, 1980), the "noise level" through which the waves are detected, and the excitation of the waves. The latter point is still an open question. Some investigators, such as Geisler and Dickinson (1976) and Madden (1978), have written that normal modes may be excited by random forcing. Charney and Strauss (1980) have proposed that normal modes

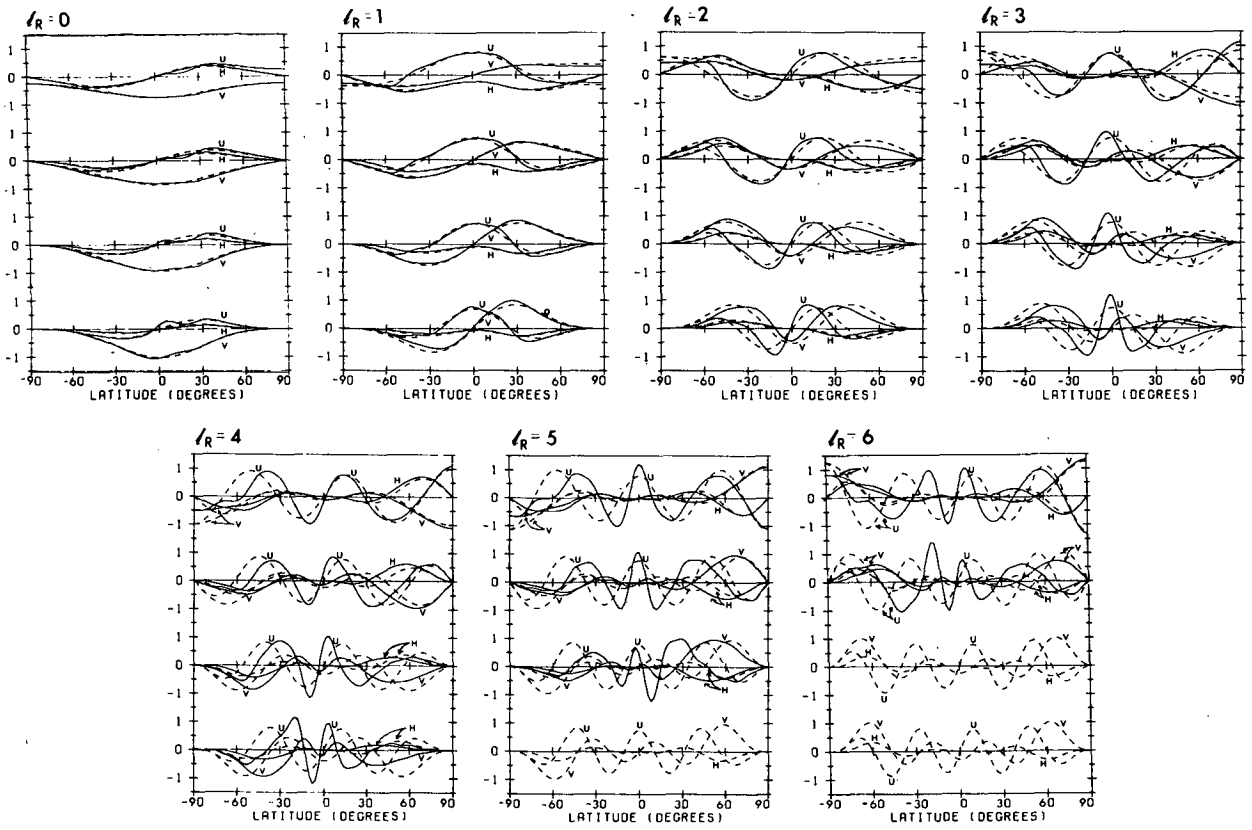

FIG. 1. Latitudinal structure of normal modes with and without the zonal wind effect. Dashed lines represent the structure in the case of no zonal flow; these are Hough functions. Solid lines represent the structure in the case of Kasahara's zonally averaged 500 mb DJF profile. The block of four graphs for each meridional index, l_R, is for zonal wavenumber $s = 1$ (at the top of each set) through $s = 4$ (at the bottom).

may be excited by the instability of orographically forced stationary waves.

4. Observational search for normal-mode Rossby waves

a. The data set

The data which were searched for normal-mode Rossby waves are the global operational analyses produced at the United States National Meteorological Center (NMC). The National Center for Atmospheric Research (NCAR) has a copy of these analyses for 0000 and 1200 GMT from 1 July 1976 to the present. The data used in this study are analyses for 0000 and 1200 GMT from 1 July 1976–13 October 1979. This is a total of 2400 analysis periods.

The NMC data set has been described briefly by Jenne (1975). The Flattery method (Flattery, 1971) using Rossby-wave Hough functions as north–south expansion functions was exclusively used to create the analyses prior to September 1978. Beginning in September 1978, the optimal interpolation (OI) method (Bergman, 1979; McPherson *et al.*, 1979) became the primary means of creating the global analyses, although occasional Flattery analyses appear in NCAR's archive after this date. The specialized time series created by the methods of the next subsection showed no discontinuities at the point when the OI method supplanted the Flattery method.

b. Creating complex time series from the data set

Eliasen and Machenhauer (1965) studied wave amplitudes and phases determined by separately projecting 500 and 1000 mb streamfunctions for the Northern Hemisphere onto theoretical Rossby wave structures. The present study followed a conceptually similar but expanded procedure, which exploited the three-dimensional, multi-variable nature of the NMC analyses. Time series were formed by projecting global three-dimensional analyses involving both geopotential and velocity onto Rossby modes of a resting isothermal atmosphere of 10 km equivalent depth (see Kasahara, 1976).

The vertical dependence of velocity and geopotential for such waves is proportional to $(p_{00}/p)^{R/c_p}$, where p_{00} is a reference pressure. Salby (1979) has shown that this so-called Lamb structure is only weakly affected when a realistic vertical temperature

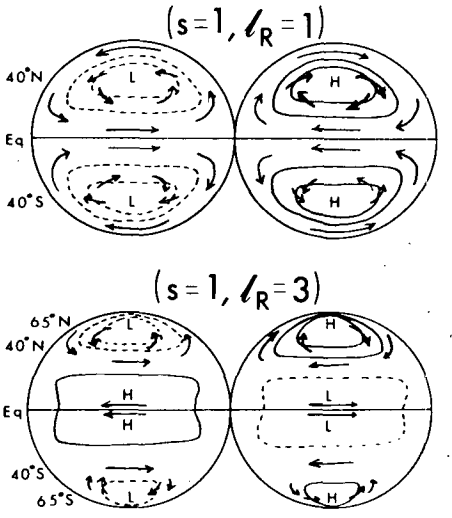

FIG. 2. Schematic view of the global geopotential and velocity fields for the generalized Laplace tidal equation modes ($s = 1$, $l_R = 1$) and ($s = 1$, $l_R = 3$) whose north-south structures are graphed in Fig. 1. "L" and "H" indicate low and high pressure centers, respectively.

profile is substituted for an isothermal one.[2] Further, Madden (1978) has found that the observed tropospheric vertical structures of the ($s = 1$, $l_R = 1$) and ($s = 1$, $l_R = 3$) modes are close to the Lamb structure.

The longitudinal dependence of our idealized free Rossby-wave structures is a sinusoid, and the latitudinal dependence is a vector Hough function. Recall from section 3 that the free Rossby-mode solutions to the generalized Laplace tidal equation are nearly Hough functions when $s + l_R$ is small, and that this result is only weakly dependent on the basic state. By using Hough functions, we avoid the difficult question of what the most realistic basic state might be for use with the generalized Laplace tidal equation. Hough functions should be sufficiently realistic for the purposes of this broad survey.

Thus, the NMC velocity and geopotential height analyses were expanded in the subspace

$$\mathrm{Re}\{\sum_{s,l} W_l^s(t)(p_{00}/p)^{R/c_p}\mathbf{H}_l^s e^{is\lambda}\}, \qquad (10)$$

where $W_l^s(t)$ is a complex time series, $p_{00} = 1000$ mb, and

$$\mathbf{H}_l^s \equiv \begin{bmatrix} (gh_e)^{1/2} & U_l^s(\theta) \\ -i\ (gh_e)^{1/2} & V_l^s(\theta) \\ h_e & H_l^s(\theta) \end{bmatrix}, \qquad (11)$$

$\mathbf{H}_l^s$ being the dimensional vector Hough function indexed by (s, l_R). The expansion of the NMC analyses was performed as follows. The Lamb mode structure was least-squares fitted to the analyses at 850, 500, and 200 mb. The expansion in longitude was performed using a fast Fourier transform. The projection onto vector Hough functions used the inner product, (5), with $H_0 = 1$, numerically integrated by Simpson's rule with data from each 10° of colatitude.

Any missing time series value $W_l^s(t)$ was filled in with the value from the preceding observation time; 2.7% of the 2400 possible observations were missing from each time series.

c. *Estimating the spectra of the complex time series*

Gonella (1972) and Mooers (1973) have discussed spectral analysis of complex time series under the name of rotary-spectral analysis. However, we prefer an approach which is a direct outgrowth of the periodogram method of spectral estimation for real time series. The periodogram method is based on the Wiener-Khinchin theorem, which also holds for complex time series. [To verify this, the reader can generalize the formal proof given by Blackman and Tukey (1958, pp. 87–88)].

The periodogram is defined as

$$P(f) = \frac{1}{N\Delta t}\left|\sum_{n=0}^{N-1}[W(n\Delta t) - \mu_W] \times \exp(-i2\pi f n\Delta t)\Delta t\right|^2, \qquad (12)$$

where f is frequency in cycles per day, N is the number of observations, Δt is the time increment in days between observations, and μ_W is the time mean of the complex time series $W(t)$. The summation may be computed at discrete frequencies $f_k = k\Delta f$, where k is an integer and $\Delta f = 1/(N\Delta t)$, using a fast Fourier transform. A periodogram for a complex time series is governed by the same theorems which apply to a periodogram for a real time series, except that the principal alias frequency interval (with frequency units of cycles per time unit) is $(-0.5/\Delta t, 0.5/\Delta t)$ for a complex time series versus $(0, 0.5/\Delta t)$ for a real time series. Periodograms for real time series have been discussed by Bloomfield (1976), Han-

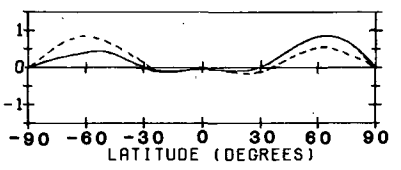

FIG. 3. Latitudinal structure of the geopotential of the ($s = 1$, $l_R = 3$) Rossby mode. The solid line is the geopotential given the DJF basic state. The dashed line is the geopotential given the JJA basic state.

[2] Later theoretical work by Salby (1980) indicates that dissipation may play an important role in altering vertical structure away from $(p_{00}/p)^{R/c_p}$, particularly in the stratosphere and above and particularly for waves with a moderate to large meridional index l_R. See also the non-Lamb structure for the ($s = 1$, $l_R = 3$) Rossby mode produced by Schoeberl and Clark's (1980) model.

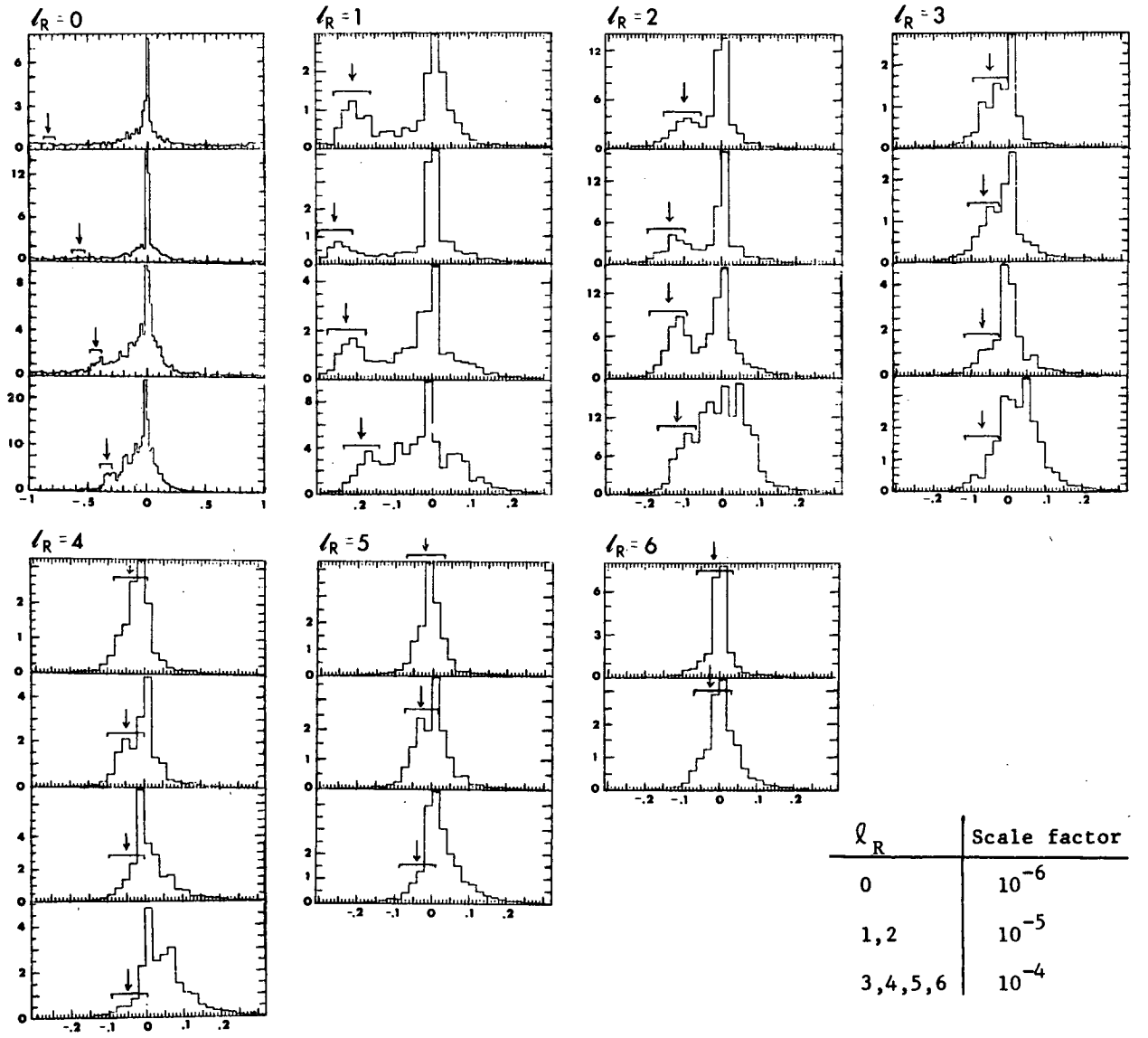

FIG. 4. Estimated spectra for the Hough function projection time series. The block of four spectra for each meridional index, l_R, is for zonal wavenumber $s = 1$ (at the top of each set) through $s = 4$ (at the bottom). Abcissa values are frequencies in units of cycles day^{-1}; negative (positive) frequencies indicate westward (eastward) moving disturbances. Ordinate values should be multiplied by the appropriate scale factor shown above and are spectral densities in units of (nondimensional variance) (cycles day^{-1})$^{-1}$. Theoretically predicted normal mode frequencies are marked by arrows. The bracket beneath each arrow is the 0.1 cycle day^{-1} wide window used in the significance test.

nan (1960), and Jenkins and Watts (1968), among others.

A smoothed or averaged version of the periodogram is an estimate of the spectrum. Fig. 4 contains the estimated spectra for the time series generated by the projection process outlined in subsection b. Each spectrum was estimated by averaging across nonoverlapping sets of 24 discrete frequencies within the periodogram. Thus, the spectral estimates are not given as continuous functions of frequency but rather are estimates of the average spectral density contained in frequency intervals of width $24\ \Delta f = 0.02$ cycles day^{-1}.

A priori, the author decided to test the spectrum of the (s, l_R) mode for a significant peak within a window 0.1 cycles day^{-1} wide centered about the theoretical frequency of the (s, l_R) mode listed in Table 1. Although the frequencies in Table 1 were computed given the DJF basic state, they differ from frequencies computed given other tropospheric basic states by much less than the window width of 0.1 cycles day^{-1}. (See Kasahara, 1980, Table 1.) The

TABLE 3. Normal mode Rossby waves detected in the spectra of Fig. 4. For each detected mode (s, l_R) there are four lines of numbers. The first line contains the approximate period range in days, determined by visually estimating the minimum and maximum frequency of the spectral peak and taking the inverse. The number in the second row for each detected mode should be multiplied by 10^{-4} and is the wave's average nondimensional amplitude at 1000 mb, corresponding to the magnitude of W_0 in (3). A question mark following a wave amplitude means that it was subjectively determined and is therefore less trustworthy. (See Section 4.d in the text regarding the computation of the wave amplitude.) Using the wave amplitude and the Hough function information in Fig. 1, the third and fourth rows were computed. The number in the third row is the wave's surface pressure amplitude in mb at the latitude where the amplitude is largest. (The surface is taken to be at a mean pressure of 1000 mb, and the pressure amplitude was computed assuming that a 1 mb disturbance at the surface corresponds to a geopotential fluctuation at 1000 mb of 8 gpm.) The number in the fourth row is the surface wind speed amplitude in m s^{-1} at the latitude where the wind speed amplitude is greatest.

The values for the waves (s = 1, l_R = 1) and (s = 1, l_R = 3) are boxed in solid lines. They are the five and 16-day waves described in Madden and Julian (1972, 1973) and Madden (1978).

s	l_R = 0	1	2	3	4	5	6
1		4–6	7.5–20	12–30			
		8	9	20 (?)			
		0.5	0.6	2.			
		0.2	0.2	0.6			
2		3.5–5	6–13	10–30	12–30	17–50	
		5	13	16 (?)	27 (?)	27 (?)	
		0.3	0.6	1.	2.	2.	
		0.1	0.3	0.5	0.7	0.7	
3	2–2.5	4–5.5	6–14				
	2	9	17				
	0.05	0.4	0.6				
	0.06	0.2	0.4				
4	3–3.5	5–7.5	6–14				
	3	10 (?)	?				
	0.05	0.3	?				
	0.09	0.3	?				

window width was chosen after checking the approximate width of peaks in the spectra computed by Madden (1978).

The null hypothesis was that the spectrum is constant across the 0.1 cycles day^{-1} interval and that this constant is the average of the spectral estimates across $3(24\Delta f)$ = 0.06 cycles day^{-1} below the test window and 0.06 cycles day^{-1} above the test window. To perform the significance test, the null hypothesis spectral density was compared to the average spectral density within the window, which has 2(0.1 cycles day^{-1})/Δf = 240 degrees of freedom. The null hypothesis was rejected if there was less than a 1% chance that it was true. Using the procedure in Bloomfield (1976, p. 196) and the asymptotic chi-square formula in Panofsky and Brier (1963, p. 55), the null hypothesis was rejected if the average spectral density within the window exceeded 1.2 times the density associated with the null hypothesis.

The frequencies from Table 1 are marked by arrows in Fig. 4. Beneath each arrow is a bracket of width 0.1 cycles day^{-1}. The significance test was particularly important for the (s = 3, l_R = 0) and (s = 4, l_R = 0) modes, which are mixed Rossby-gravity waves. The small peaks at the theoretically predicted frequencies pass the stated significance test, but the peaks almost certainly would have been overlooked if the wave frequencies and the peak width had not been specified *a priori*.

All the spectra show a red-noise character, and this made it impossible to apply the significance test in those cases where the peak frequency was not well-separated from the red noise peak at f = 0. In such instances, any normal mode would be inextricably merged with the red-noise spectrum, and the only evidence for the presence of a normal mode peak would be asymmetry in the peak about f = 0. Of course, asymmetry in the red noise peak about f = 0 could be due to other factors than normal modes, but the red-noise peaks do tend to be fairly symmetric in those spectra having normal mode peaks which are not near f = 0.

d. Interpretation of the estimated spectra

Probably the most important fact to bear in mind when examining the spectral estimates in Fig. 4 is that the spectra were produced from global weather analyses, each of which is a complicated merging and smoothing of atmospheric observations with an NMC global computer forecast. Because computer forecasts are not perfect, it would be hasty to conclude that the spectral estimates in Fig. 4 necessarily apply to the real atmosphere without alteration. For now, all that can be said is that the spectra apply to the global operational analyses produced by the National Meteorological Center.

As summarized in Table 3, the existence of somewhere between 8 and 14 normal modes is indicated by the spectra in Fig. 4. Spectral peaks for all four of the l_R = 1 modes and for three of the four l_R = 2 modes clearly pass the significance test. Only two l_R = 0 modes pass the significance test, and they only barely pass. The remaining modes listed in Table 3 were not tested for significance because of the red-noise problem mentioned earlier; however, in the opinion of the author, spectral peaks seem to exist within the test windows for these modes. In Table 3, their estimated amplitudes are followed by question marks to indicate their speculative nature. These amplitudes were estimated by assuming that the red-noise spectrum should be symmetric about f = 0 in the absence of a spectral peak and by ascribing to each normal mode the variance which exceeds that due to symmetry.

The amplitudes in Table 3 apply to idealized Rossby-mode structures and therefore may be only approximately correct for actual free modes in the

atmosphere. For example, there are likely to be seasonal hemispheric asymmetries, as suggested by Fig. 3 and as more fully explored by Geisler and Dickinson (1976) and Schoeberl and Clark (1980). This is almost certainly part of the reason why the 2 mb average amplitude estimated here for the ($s = 1$, $l_R = 3$) wave is less than the 5 mb winter amplitude obtained by extrapolating Madden's (1978, Fig. 7) measurements to 1000 mb. Other possible reasons for our amplitude being different from Madden's are interannual variability (Sato, 1977) and our use of a global projection process, which would give underestimates if the NMC analyses show insufficient Southern Hemisphere variability due to sparse observations.

Haurwitz's study (1940) was motivated by the conjecture that the strength of the Icelandic and Aleutian lows and the Pacific and Azores highs might be partly due to resonance with the ($s = 2$, $l_R = 3$) normal mode. The spectral analysis in Fig. 3 does not indicate an especially large amplitude for this wave, so evidence does not favor Haurwitz's hypothesis.

Pratt and Wallace (1976) reported tropospheric evidence of a zonal wavenumber-two, westward-propagating wave which had a ~20 day period. Vertically, there was little tilt, and amplitude increased with height. At the three latitudes at which data were analyzed, 40, 50, and 60°N, amplitude was maximum at 60°N. The vertical structure information suggests that the wave is a free mode. The period and the latitudinal structure, when checked against Table 1 and Fig. 1, suggest that the wave may be the ($s = 2$, $l_R = 4$) mode.

Eliasen and Machenhauer (1965) tentatively identified the ($s = 3$, $l_R = 3$) Rossby mode, but our spectrum for that mode does not boast a convincing peak at the theoretical frequency. Eliasen and Machenhauer expanded only Northern Hemisphere streamfunctions and so used only symmetric associated Legendre polynomials for latitudinal expansions. Thus, their hemispheric projection for ($s = 3$, $l_R = 3$) may have been contaminated by the ($s = 3$, $l_R = 2$) mode, which our study did detect. The question of the existence of the ($s = 3$, $l_R = 3$) mode requires further investigation.

The seasonal dependences of the spectra have not yet been estimated extensively, but preliminary checks indicate that the variance is generally larger in the December–February period than during June–August. The spring and autumn periods have an intermediate amount of variance. Seasonal variability is related to the question of stationarity of the time series (Salby, 1980), and the author has begun an observational check into this matter.

It is intriguing to consider the spectra for ($s = 4$, $l_R = 3$) and ($s = 4$, $l_R = 4$). There is definitely more power traveling eastward than westward for these modes; in fact, there are distinct peaks at eastward frequencies. Eliasen and Machenhauer (1969, Table 4) also observed eastward motion for modes with $s + l_R \geq 7$. Their observed eastward wave speeds matched well with theoretical speeds computed assuming a basic state in solid body rotation. However, realistic basic states possess both easterly and westerly winds, and such basic states do not have free Rossby modes that travel eastward in the discrete spectrum (see Kasahara, 1980, Section 7). How is it, then, that an unrealistic model does such a good job of predicting wave speeds for large $s + l_R$? Is this just chance? The author does not know. It should also be pointed out that Schoeberl and Clark's (1980) linear model exhibited resonant responses at eastward-moving frequencies.

5. Summary

In Section 3, we saw that the structure of a free Rossby mode in a global shallow water model is not altered significantly by adding a moving basic state, provided $s + l_R$ is small. This near constancy of structure motivated the spatial filtering process used to look for these theoretical modes. Nonetheless, the chosen Lamb mode/Hough function structures are highly idealized, as more complicated modeling efforts by Geisler and Dickinson (1976), Schoeberl and Clark (1980), and Salby (1980) have shown.

Spectral analyses of complex time series representing amplitudes and phases revealed that considerably more than the two previously documented normal modes are evident in the NMC global analyses. The periods of these waves range from ~2 to ~30 days. This is the time scale over which many fluctuations in weather occur, but this study has not found normal modes to be strongly excited. Indeed, the spectra of Fig. 4 show that, even after spatial filtering, red noise is more prominent than the quasi-periodic components.

Recent work by Daley *et al.* (1981) has demonstrated that numerical models with hemispheric domains or with inaccurate initial data from the tropics exhibit overly strong free Rossby-mode responses. The amplitudes of these waves are sufficiently large that they cause significant degradation of forecast skill. The lesson seems to be that normal mode concepts are useful for initializing and diagnosing numerical models but that normal modes themselves do not figure prominently in the atmospheric response.

Acknowledgments. The author thanks J. Kutzbach, T. Starr, A. Kasahara, M. Salby, R. Madden, J. Young, D. Houghton, D. Johnson, K. Weickmann and an anonymous reviewer for their criticism and suggestions. This research was sponsored by National Science Foundation grants ATM-74-23041 and ATM-79-26039 and by a computer resources

grant from the National Center for Atmospheric Research, which is sponsored by the National Science Foundation.

REFERENCES

Bergman, K., 1979: Multivariate analysis of temperatures and winds using optimum interpolation. *Mon. Wea. Rev.*, **107,** 1423–1444.

Blackman, R., and J. Tukey, 1958: *The Measurement of Power Spectra.* Dover, 190 pp.

Bloomfield, P., 1976: *Fourier Analysis of Time Series.* Wiley, 258 pp.

Boyd, J., 1978: The choice of spectral functions on a sphere for boundary and eigenvalue problems: a comparison of Chebyshev, Fourier, and associated Legendre expansions. *Mon. Wea. Rev.*, **106,** 1184–1191.

Burpee, R., 1976: Some features of global-scale 4–5 day waves. *J. Atmos. Sci.*, **33,** 2292–2299.

Charney, J., and D. Strauss, 1980: Form-drag instability, multiple equilibria and propagating waves in baroclinic, orographically forced, planetary wave systems. *J. Atmos. Sci.*, **37,** 1157–1176.

Daley, R., 1981: Normal mode initialization. *Rev. Geophys. Space Phys.*, **19,** 450–468.

——, J. Tribbia and D. Williamson, 1981: The excitation of large-scale free Rossby waves in numerical weather prediction. *Mon. Wea. Rev.*, **109,** 1836–1861.

Dickinson, R., and D. Williamson, 1972: Free oscillations of a discrete stratified fluid with application to numerical weather prediction. *J. Atmos. Sci.*, **29,** 623–640.

Dikii, L., and G. Golitsyn, 1968: Calculation of the Rossby wave velocities in the Earth's atmosphere. *Tellus*, **20,** 314–317.

Eliasen, E., and B. Machenhauer, 1965: A study of the fluctuations of the atmospheric flow patterns represented by spherical harmonics. *Tellus*, **17,** 220–238.

——, and ——, 1969: On the observed large-scale atmospheric wave motions. *Tellus*, **21,** 149–165.

Flattery, T., 1971: Spectral models for global analysis and forecasting. *Proc. Sixth AWS Technical Exchange Conf.*, U.S. Naval Academy, Air Weather Service Tech. Rep. 242, 42–53.

Geisler, J., and R. Dickinson, 1976: The five-day wave with realistic zonal winds. *J. Atmos. Sci.*, **33,** 632–641.

Gonella, J., 1972: A rotary-component method for analyzing meteorological and oceanographic vector time series. *Deep-Sea Res.*, **19,** 833–846.

Hannan, E., 1960: *Time Series Analysis.* Wiley, 152 pp.

Haurwitz, B., 1940: The motion of atmospheric disturbances on the spherical Earth. *J. Mar. Res.*, **3,** 254–267.

Jenkins, G., and D. Watts, 1968: *Spectral Analysis and its Applications.* Holden-Day, 525 pp.

Jenne, R., 1975: Data sets for meteorological research. NCAR Tech. Note, NCAR-TN/IA-111, 194 pp.

Kasahara, A., 1976: Normal modes of ultralong waves in the atmosphere. *Mon. Wea. Rev.*, **104,** 669–690.

——, 1980: Effect of zonal flows on the free oscillations of a barotropic atmosphere. *J. Atmos. Sci.*, **37,** 917–929.

——, 1981: Corrigendum. *J. Atmos. Sci*, **38,** 2284–2285.

Longuet-Higgins, M., 1968: The eigenfunctions of Laplace's tidal equations over a sphere. *Phil. Trans. Roy. Soc. London*, **A262,** 511–607.

Madden, R., 1978: Further evidence of traveling planetary waves. *J. Atmos. Sci.*, **35,** 1605–1618.

——, 1979: Observations of large-scale traveling Rossby waves. *Rev. Geophys. Space Phys.*, **17,** 1935–1949.

——, and P. Julian, 1972: Further evidence of global-scale 5-day pressure waves. *J. Atmos. Sci.*, **29,** 1464–1469.

——, and ——, 1973: Reply to comments by R. J. Deland. *J. Atmos. Sci.*, **30,** 935–940.

McPherson, R., K. Bergman, R. Kistler, G. Rasch and D. Gordon, 1979: The NMC operational global data assimilation system. *Mon. Wea. Rev.*, **107,** 1445–1461.

Mooers, C., 1973: A technique for the cospectrum analysis of pairs of complex-valued time series with emphasis on properties of polarized components and rotational invariants. *Deep-Sea Res.*, **20,** 1129–1141.

Moura, A., 1976: The eigensolution of linearized balance equations over a sphere. *J. Atmos. Sci.*, **33,** 877–907.

Orszag, S., 1974: Fourier series on spheres. *Mon. Wea. Rev.*, **102,** 56–75.

Panofsky, H., and G. Brier, 1963: *Some Applications of Statistics to Meteorology.* The Pennsylvania State University, 224 pp.

Pratt, R., and J. Wallace, 1976: Zonal propagation characteristics of large-scale fluctuations in the midlatitude troposphere. *J. Atmos. Sci.*, **33,** 1184–1194.

Salby, M., 1979: On the solution of the vertical structure problem for long-period oscillations. *J. Atmos. Sci.*, **36,** 2350–2359.

——, 1980: The influence of realistic dissipation on planetary normal structures. *J. Atmos. Sci.*, **37,** 2186–2199.

Sato, Y., 1977: Transient planetary waves in the winter stratosphere. *J. Meteor. Soc. Japan*, **55,** 89–105.

Schoeberl, M., and J. Clark, 1980: Resonant planetary waves in a spherical atmosphere. *J. Atmos. Sci.*, **37,** 20–28.

Yanai, M., J.-H. Chu, T. Stark and T. Nitta, 1976: Response of deep and shallow tropical maritime cumuli to large-scale processes. *J. Atmos. Sci.*, **33,** 976–991.